JOURNAL OF AIRCRAFT
Vol. 43, No. 6, November–December 2006

Simulation of Soft Projectiles Impacting Composite Targets using an Arbitrary Lagrangian–Eulerian Formulation

Jingyun Cheng* and Wieslaw K. Binienda†
University of Akron, Akron, Ohio 44325-3905

DOI: 10.2514/1.19425

Methods for modeling the impact of triaxial braided composites with a gelatin projectile have been developed using the commercial explicit finite element code LSDYNA. An arbitrary Lagrangian–Eulerian formulation was used to resolve problems with numerical instability that were encountered in previous simulations based on a pure Lagrangian formulation. The LSDYNA MAT 58 material model and shell elements were used for the composite. Composite material properties were obtained from available experimental data and micromechanics calculations. The impact dynamics and penetration thresholds observed in the experiments were adequately simulated. The simulated contact forces between the projectile and composite material were useful for understanding the onset of penetration. The effect of boundary conditions on the penetration threshold was simulated using spring elements located at the boundaries. Simulations confirmed experimental observations that the penetration threshold is higher when slipping occurs during the impact. The impact simulations also show that the reaction forces at the boundaries of the half-ring are much smaller than for the flat plates, and so the boundary slipping will occur more likely during the flat plate impact case.

I. Introduction

RECENT experimental results have indicated that carbon fiber/epoxy composites with a triaxial braid fiber architecture are resistant to cracking and delamination during impact [1]. In these experiments, composite plates and half-rings were impacted with a soft gelatin projectile. Damage began as fiber tensile failure in the back ply at low-impact velocities. As the impact velocity was increased above the penetration threshold, cracks grew from the initial damage site in preferred directions along the fiber bundles. The cracks propagated only a small distance away from the impact site, and no delamination was observed.

Preliminary simulations of these experiments were performed [2] using the explicit finite element code, LSDYNA [3]. In this previous work, a Lagrangian formulation was used with the equation of state (EOS) material model for the gelatin projectile. Material properties for the gelatin were adjusted so that results of the simulations correlated well with the experimental results. Using this approach, it was possible to simulate the overall impact dynamics, the damage initiation threshold, and the penetration threshold. However, two improvements are needed for these simulations. First, improvements in the composite material model are needed to fully account for the effect of fiber architecture on the direction and extent of crack propagation. Second, a more robust material model is needed for the gelatin projectile. In this paper, an alternative approach for modeling the projectile is reported. Improvements to the composite model will be reported elsewhere.

As stated in the preceding paragraph, material properties for the gelatin projectile were adjusted to match numerical results with experimental results. A more robust approach would be to use measured material properties for the material model. However, this approach is not feasible because material properties for the gelatin material at strains and strain rates representative of conditions in the experiments are not available and not easily measured. An alternative approach is to perform a separate set of impact tests using the same projectile material and a rigid target instrumented for force measurements. Material properties can then be extracted by matching results of the simulations with the transient force measurements during impact. Transient force measurements for cylindrical gelatin projectiles impacting a rigid target have been reported by Wilbeck [4]. An initial attempt to simulate these experiments using the Lagrangian formulation in LSDYNA was not successful. Although the Lagrangian formulation was used successfully to simulate impact against the compliant composite targets used in [1], numerical instabilities occurred when the same method was used to simulate impact against the rigid targets used in [4]. One source of the instability was severe mesh distortion near the contact surface early in the simulation. An alternative approach is to use an Eulerian formulation. In an Eulerian formulation, material flows though a fixed mesh, so mesh distortion is not a problem. An arbitrary Lagrangian–Eulerian (ALE) formulation is available in LSDYNA [5]. The ALE formulation allows an Eulerian formulation to be used for the projectile model and a Lagrangian formulation to be used for the target model. In this paper, the ALE formulation is used to simulate the experimental results in [4]. Material properties extracted from these simulations are then used for the material model in simulations of the composite impact tests in [1].

II. Experimental Results

Information from previous experimental work that is needed for correlation with the numerical simulations reported in this paper is briefly reviewed here. Further details about the impact tests can be found in [1] for the composite targets and in [4] for the rigid targets. The projectiles used for the impact tests with composite targets were made by casting a mixture of gelatin and microballoons into the shape of a cylinder 12.7-cm-long and 7.0 cm in diameter. The density of the solidified projectiles was 960 kg/m^3. Figure 1 shows an example of a projectile before, during, and after impact. During a test, the projectile initially flattens into a pancake shape before either rebounding or perforating the composite target. At low velocities, the projectile can be recovered completely undamaged, and at high velocities, the projectile is disintegrated into small pieces. At intermediate velocities, the projectile rebounds to the partially damaged shape shown in Fig. 1c. The projectiles used for impact tests with the rigid target were also a mixture of gelatin and microballoons with a similar density of 950 kg/m^3. Impact

Received 10 August 2005; revision received 2 May 2006; accepted for publication 15 May 2006.

*Graduate Student, Civil Engineering Department.
†Corresponding Author, Professor, Civil Engineering Department; Wbinienda@uakron.edu.

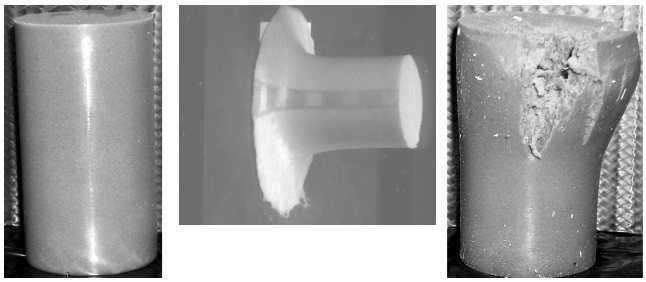

a) b) c)

Fig. 1 Gelatin projectiles a) before, b) during, and c) after impact.

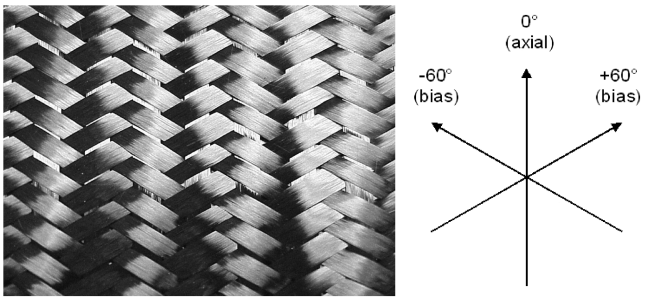

Fig. 2 0/ ± 60 deg triaxial braid architecture.

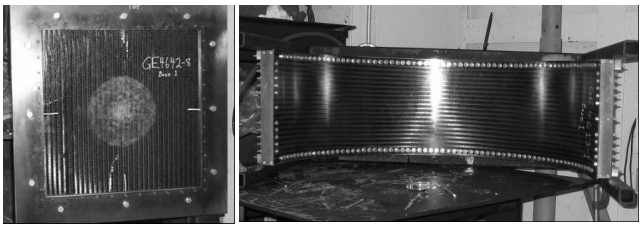

a) 56×56 cm flat plate b) 112 cm diameter half-ring

Fig. 3 Composite targets mounted in the impact test fixtures.

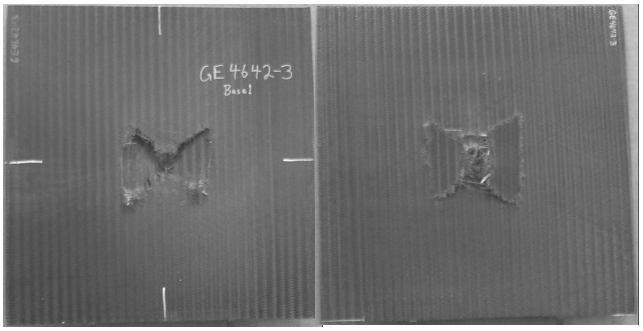

a) Front b) Back

Fig. 4 Composite plate after impact at 192 m/s.

Fig. 5 Back side of composite half-ring after impact at 150 m/s.

velocities ranged from 103 to 198 m/s for the composite targets and from 100 to 250 m/s for the rigid targets.

Composites were fabricated by infusion of epoxy resin into six layers of a carbon fiber triaxial braid preform. The axial and bias yarn directions for the 0/ ± 60 deg braid architecture are shown in Fig. 2. Because of the 0/ ± 60 deg braid architecture, the six-ply composite is quasi-isotropic both globally and within each ply. The cured composites had a thickness of about 3.2 mm. Composites were fabricated in the form of 56 × 56 cm flat plates and 112-cm-diam half-rings. The composite targets are shown mounted in the test fixtures in Figs. 3a and 3b.

The first set of composite impact tests was performed on eight flat plates with impact velocities ranging from 103 to 198 m/s. The penetration threshold was between 150 and 161 m/s. Figure 4 shows the front and back surfaces of the composite plate tested at 192 m/s. Failure is initiated at the center of the plate on the back side where the tensile strain reaches the failure strain of the composite. Cracks then propagate along the ±60 deg bias fiber directions. When these cracks extend beyond the initial contact area, triangular flaps fold back along the zero degree axial fibers. The cracks do not propagate far from the initial impact area and there is no apparent delamination between plies. The flat plates were more difficult to test than the half-rings because the edges of the plates had a tendency to slip in the fixture, especially at impact velocities approaching the penetration threshold. Slipping at the boundaries was not observed at the boundaries of the half-ring fixtures.

Two composite half-rings were tested using the fixture shown in Fig. 3b. The zero degree fibers are oriented circumferentially in the half-ring. Because the damage was localized, it was possible to perform three separate impact tests on each half-ring. One impact site was at the center and the other two impact sites were at side locations between the center and the ends of the half-ring. Assumptions behind this experimental approach are that 1) the penetration threshold is not affected by the different boundary conditions at the center and side locations, and 2) the penetration threshold is not affected by damage from prior impact tests. The first assumption is evaluated analytically later in this paper. The second assumption is currently being investigated. Six tests were performed with impact velocities ranging from 107 to 150 m/s. The penetration threshold was between 133 and 138 m/s. For velocities above the damage threshold but below the penetration threshold, a small circular region of fiber fracture occurred in the back ply directly behind the center of the initial impact area, similar to the initial damage mode for the flat plates. Also similar to the flat plates, the region of fiber fracture is the initiation site for crack propagation when the impact velocity exceeds the penetration threshold. However, the crack pattern for the half-rings (Fig. 5) is different from that for the flat plates (Fig. 4). In the half-rings, the cracks propagate from the initiation site in a direction transverse to the zero degree fibers (axial direction for the half-ring) rather than along a fiber direction. As the cracks reach locations near edges of the initial impact site, each of the transverse cracks split into two cracks that travel a short distance along the ±60 deg fiber directions. These cracks then turn again to travel along the zero degree fibers. Square flaps then open by folding along a line transverse to the zero degree fibers. The final damage area is slightly larger than the initial contact area.

III. Finite Element Model

A. Background

Wilbeck gave a comprehensive description of the impact of a soft cylindrical projectile against a rigid plate [4]. When the soft projectile

impacts the target, a shock wave is formed when particles on the front surface of the projectile are instantaneously brought to rest relative to the target. The pressure in the shock region is very high initially and is constant throughout the shock region. As the shock propagates, a complicated stress field with high pressure gradients develops in the projectile. If, at any time, the state of stress exceeds the strength of the material, the material "flows" like a fluid. After several reflections of the stress waves, a condition of steady flow is established. Constant pressure and velocity fields are then established in the projectile. At this stage, the contact pressure is lower than the initial peak pressure.

The initial contact pressure is called the Hugoniot pressure. For a soft projectile impacting a rigid (incompressible) target, the Hugoniot pressure can be described as

$$P = \rho_1 u_s u_0 \tag{1}$$

where ρ_1 is the density of the projectile, u_s is the shock wave velocity, and $u_o$is the projectile's initial velocity.

For a soft projectile impacting a nonrigid (compressible) target, the Hugoniot pressure can be described as

$$P = \rho_p u_{\mathrm{sp}} u_0 \left(\frac{\rho_t u_{\mathrm{st}}}{\rho_p u_{\mathrm{sp}} + \rho_t u_{\mathrm{st}}} \right) \tag{2}$$

where ρ_p is the density of the projectile, ρ_t is the density of the target, u_{sp} is the projectile shock wave velocity, u_{st} is the target shock wave velocity, and u_o is the projectile's initial velocity. In Eqs. (1) and (2), the initial peak pressure depends only on densities and velocities and not on the length or cross-sectional area of the projectile. These equations describe only the initial pressure and not the pressure in the steady flow region. Numerical simulations are needed to calculate pressure in the steady flow region and to include the effects of structural compliance of the target. The transient force measurements in [4] show an initial force peak followed by an approximately constant pressure flow region. Material properties are extracted from numerical simulations by matching these peak and steady flow pressures.

As mentioned in the preceding section, modeling of the projectile using a conventional Lagrangian formulation was not possible because the severe mesh distortion caused numerical instability. In an explicit finite element analysis, the time step is determined by the smallest element dimension. The severe mesh distortion caused the time step to decrease to an unacceptably low value for the calculations to continue. In a pure Eulerian description, material moves through the mesh and there is no element distortion. The ALE formulation in LSDYNA contains both Lagrangian and Eulerian formulations and captures the advantages of both Lagrangian and Eulerian finite elements. The ALE approach is based on the arbitrary movement of a reference domain [5]. In this paper, the ALE formulation in LSDYNA was used. The soft gelatin projectile was modeled with a multimaterial Eulerian formulation, whereas the composite target was modeled with a Lagrangian formulation.

B. Projectile Model

Because the gelatin has a very low strength and stiffness, it can be described using the LSDYNA Material 9 (MAT_NULL), in which the pressure–volume relation is modeled using the equation of state. This material model uses the equation of state without computing deviatoric stresses. The linear polynomial form available in LSDYNA is

$$P = C_0 + C_1 \propto + C_2 \propto^2 + C_3 \propto^3 + (C_4 + C_5 \propto + C_6 \propto^2) E \tag{3}$$

where $\propto = \frac{\rho}{\rho_0} - 1$, $\frac{\rho}{\rho_0}$ is the ratio of current density to initial density, and C_i are the material constants.

Constants C_4, C_5, and C_6 were set to zero because of the low value of Young's modulus for the soft projectile material. It is recognized that this is an oversimplification of the material model. However, the goal of this preliminary set of simulations is to evaluate the ALE formulation rather than to develop an exact material model. The material model can be refined as more instrumented impact test data and more material property data (e.g., bulk modulus, Young's modulus) become available. There is an additional consideration concerning the accuracy of the material model. It is not possible to extract accurate material property data from explicit finite element analysis of impact experiments because material properties extracted from the analyses are not unique. In explicit finite element analysis, results depend on both the material properties specified and parameters selected within the material model to ensure reasonable run time and numerical stability. For example, consider the effect of mesh density. The time step in explicit analyses is controlled by the smallest element dimension. As a result, the mesh must be defined in part to give a reasonable run time. Because results of explicit analyses depend on mesh density, material properties extracted from explicit finite element analyses of impact experiments depend on the mesh density used. Subsequent analyses are valid only when the mesh density and other model parameters are kept the same. In this paper, the material model determined using the data from [4] is used to simulate impact test results in [1], keeping the mesh size and other model parameters the same. An additional concern with explicit finite element analysis is that some amount of artificial energy dissipation is unavoidable as the simulation proceeds. After each simulation, the energy balance and the evolution of various forms of energy were examined to ensure that the level of artificial energy dissipation was not significant in the simulation.

As discussed in the preceding section, the value of C_i is determined by correlating results of numerical simulations with the peak pressures and steady flow pressures reported in [4]. Figure 6 shows the deformed projectile at different impact times in the simulation. The projectile deformation is similar to the pancakelike shape observed in the impact experiments (see Fig. 1b). Figure 7 shows a comparison of the calculated pressure at the center of the rigid plate with test data from [4]. Time and pressure are plotted in nondimensional forms obtained by dividing the time by l/V_0 (the time for an unimpeded projectile to travel a distance l at a velocity V_0) and by dividing the pressure by $0.5\rho_0 V_0^2$. The nondimensional forms are shown in Eqs. (4) and (5), where V_0 is the impact velocity, l is the projectile length, and p is the normal pressure of the center element in the rigid plate.

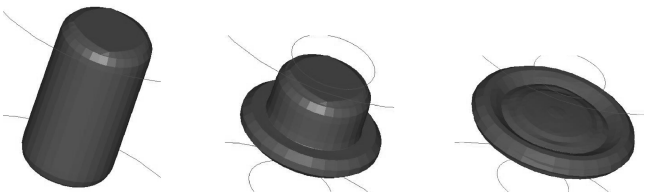

Fig. 6 ALE simulation of gelatin impact on rigid plate at 117 m/s.

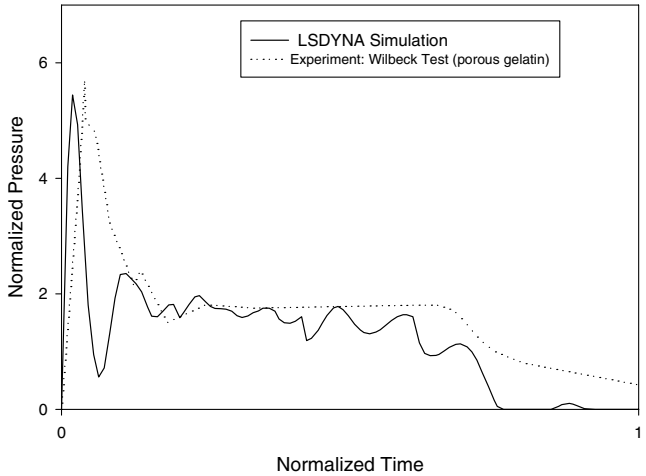

Fig. 7 Gelatin projectile impact against rigid target at 117 m/s (— simulation, ---- data from [4]).

Table 1 Material constants used in the analysis (* indicates measured properties)

Property name	Magnitude
Mass density*	1538.6, kg/m^3
Young's modulus—longitudinal direction*	45.02, GPa
Young's modulus—transverse direction*	45.57, GPa
v_{ba} Poisson's ratio ba*	0.27
Shear modulus ab*	17.79, GPa
Shear modulus bc	4.83, GPa
Shear modulus ca	17.65, GPa
Strain at longitudinal compressive strength, a-axis*	0.013
Strain at longitudinal tensile strength, a-axis*	0.017
Strain at transverse compressive strength, b-axis*	0.0099
Strain at transverse tensile strength, b-axis*	0.012
Strain at shear strength, ab plane	0.012
Longitudinal compressive strength*	506.8, MPa
Longitudinal tensile strength*	799.8, MPa
Transverse compressive strength*	421.9, MPa
Transverse tensile strength*	455.7, MPa
Shear strength, ab plane*	252.0, MPa

$$t_N = \frac{tV_0}{l} \tag{4}$$

$$P_N = \frac{p}{0.5\rho_0 V_0^2} \tag{5}$$

The values of both the peak pressure and the steady flow pressure are adequately simulated in the material model. Numerical simulations agreed with the experimentally determined peak and steady flow pressures within 10% over the entire velocity range.

C. Composite Target Model

The composite targets were modeled as 60.96×60.96 cm flat plates and 111.76-cm-diam half-rings fixed at all edges. For computational efficiency, the composite plate and half-ring were modeled using shell elements with multiple points of integration. Because of the $0/\pm 60$ deg fiber architecture, the composite is treated as a homogeneous, quasi-isotropic material. The strain rate dependence of material properties is not considered. A composite continuum damage mechanics model [6] was chosen for this work because it simulates closely the nonlinear stress-strain behavior of braided composites. This is Model 58, MAT_LAMINATED_-COMPOSITE_FABRIC, in LSDYNA. Model 58 is adequate for an approximate analysis of impact dynamics and for an estimation of the stress and strain fields within the composite at various times during impact. The model is not currently capable of simulating all failure modes in the braided composite. The properties used in the analysis are shown in Table 1. Some composite material properties were measured using test coupons cut from undamaged areas of the impacted plates [7]. These are indicated with an asterisk in Table 1.

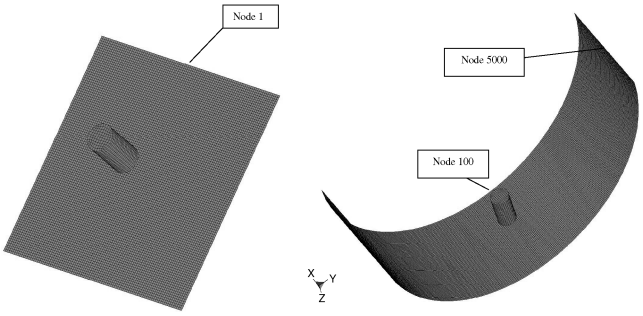

Fig. 8 Finite element meshes for plate, half-ring, and projectile.

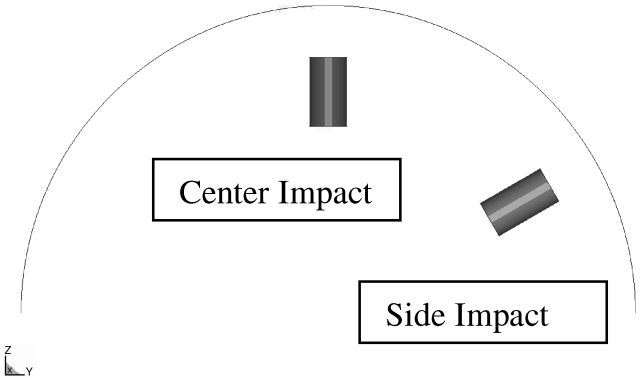

Fig. 9 Center and side impact locations for the half-ring composite target.

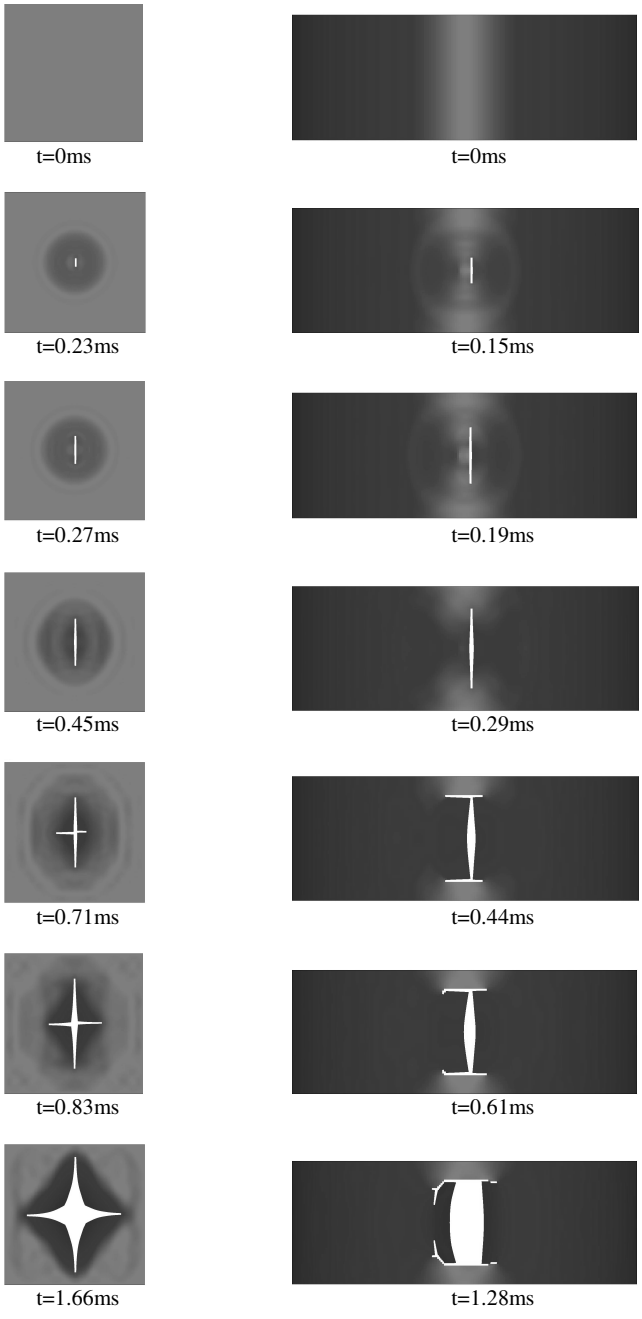

Fig. 10 Development of perforation for a) flat panel at 154 m/s, and b) half-ring at 134 m/s.

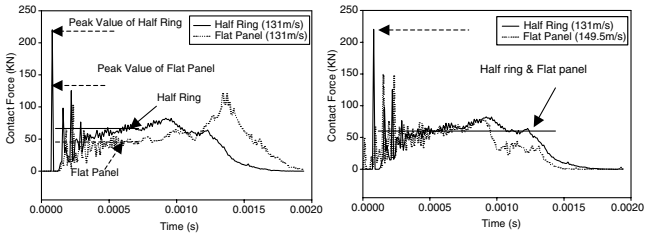

a) Equal impact velocities **b)Velocities just below the penetration threshold**

Fig. 11 Contact force comparison of the flat panel and half-ring.

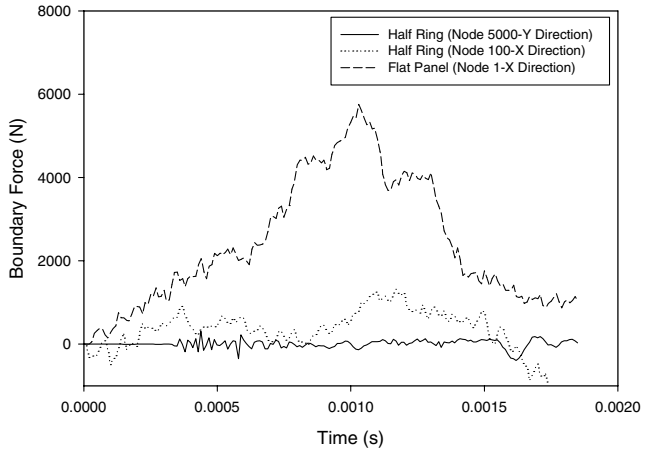

Fig. 12 Force-time history at the boundary for nodes indicated in Fig. 6 for impact at a velocity 131 m/s.

The remaining properties are assumed values based on micro-mechanics calculations.

The meshes used to model the projectile, the half-ring, and the plate are shown in Fig. 8. The plate mesh contains 10,000 elements, and the half-ring mesh contains 23,214 elements. The half-cylinder and plate are rigidly fixed at all edges. To simulate the slipping of targets in the impact test fixture that was observed in some tests, elastic perfectly plastic spring elements were used to allow motion and simulate friction at the boundaries. The specific nodes identified in Fig. 8 are used for evaluating reaction forces at the boundaries. Impact simulations were performed for impact at the center locations shown in Fig. 8. The effect of impacting the half-ring at a side location, as shown in Fig. 9, is also examined.

IV. Finite Element Analysis Results

Impact of the composite plate was simulated for velocities ranging from 91.4 to 167.6 m/s. The penetration threshold for the plates was determined to be between 149.5 and 154 m/s. Impact of the composite half-rings at the center location was simulated for velocities raging from 91.4 to 152.4 m/s. The penetration threshold for the half-ring was determined to be between 131 and 134 m/s.

To determine the effect of impact location on the penetration threshold for the half-ring, simulation of side impact on the half-ring (see Fig. 9) was also conducted. Penetration occurred at a velocity of 130 m/s for the side impact, similar to the value of 131 m/s obtained for central impact. This supports the experimental assumption that results of central and side impacts are similar for previously undamaged half-ring targets. The effect of preexisting damage at adjacent sites is still under investigation.

Figure 10a shows damage progression during impact of a plate at the threshold velocity of 154 m/s. The crack initiates at the center of the plate and grows symmetrically along the zero and 90 deg directions. This is different from the experimental failure pattern shown in Fig. 4 because the quasi-isotropic material model and the maximum strain failure criterion do not take into account the actual strength of the composite in all directions. Efforts are currently underway to include the effect of fiber architecture on the direction of crack propagation in the composite model. Figure 10b shows damage progression during impact of a half-ring at the threshold velocity of 134 m/s. A crack initially propagates along a direction perpendicular to the zero degree fibers. The crack then turns and propagates along the zero degree fibers. The size and shape of the damaged region are similar to the experimental results shown in Fig. 5 except that the small section of crack propagation along the 60 deg fiber direction is not present.

Figure 11 shows a comparison of contact force-time histories for the flat panel and the half-ring. In Fig. 11a the impact velocity is the same for the plate and the half-ring. For equal impact velocities, the average force is higher for the half-ring. This is a result of reduced compliance of the target due to curvature stiffness. In Fig. 11b force-time histories are compared at the penetration threshold rather than at equal impact velocities. At the penetration threshold, the average force is nearly the same for the half-ring and the plate. This is consistent with other investigations in which contact force was found to be a good parameter for scaling of impact test results [8,9].

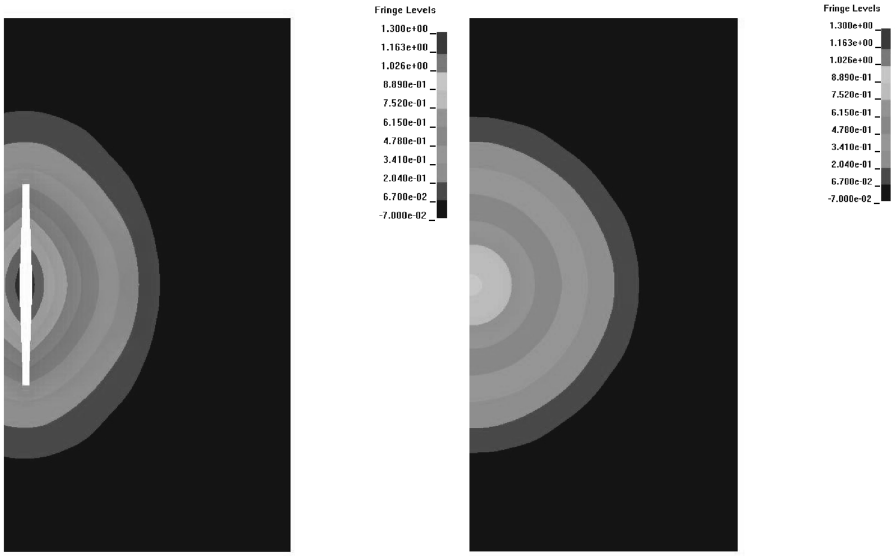

a) FEM model with fixed boundary conditions **b) FEM model with 0D spring elements**

Fig. 13 Out of plane displacement for flat panel impact (117 m/s).

To investigate the effect of slipping of the target in the fixture on the experimentally determined penetration threshold, boundary force-time histories were determined for an impact velocity of 131 m/s. Figure 12 compares the boundary force-time histories for the plate and for the half-ring impacted at the center impact locations identified in Fig. 8. The forces indicated in Fig. 12 are in the plane of the composite and normal to the boundary. For the half-ring, node 100 is closest to the impact site and has the largest boundary force. Node 5000 is farthest from the impact site and has a very low boundary force. For the flat panel, node 1 is in the middle of the plate edge boundary. The boundary forces for the plate are much larger than those for the half-ring. This explains the experimental observation that the plate has a greater tendency to slip out of the edges of the test fixture. The influence of slipping at the boundaries on the impact of the panel is illustrated in Fig. 13. Frictional boundary conditions are modeled by using elastic perfectly plastic spring elements added along the four sides of the plate. The simulations indicated that at a velocity sufficient for penetration of the fixed plate there is no penetration when the boundaries of the plate are allowed to move. As shown in Fig. 13, the impact velocity for fixed plate and plate with spring elements is 154 m/s. An important implication of these results is that laborious efforts such as drilling and pinning of panel edges to prevent slipping of the panel during the impact test may be needed to accurately determine the penetration threshold.

V. Conclusions

An explicit FEM model has been developed for the impact of triaxial braid composite plates and half cylinders with a soft projectile using LSDYNA code. The impact dynamics and penetration threshold were observed in the experiments and numerical simulations. Penetration threshold velocity for the half-ring was smaller than for the plate, but the average contact forces at these velocities were the same. The impact location does not affect the penetration threshold greatly for the half-ring. The slippage of the boundary may affect the penetration threshold at the plate as boundary reactions are much higher than in case of the half-cylinder impact.

In this simulation, the arbitrary Lagrangian–Eulerian method has been used for modeling the projectile, which partly captures the deformation and damage shape. The limit for this method exists, as this material model cannot capture the deformation and contact force during the unloading stage. Further development of material model and failure criterion are needed to fully simulate damage patterns. In particular, a strain rate dependent material model is needed for more accurate prediction of experimental results.

Acknowledgments

This work was conducted thanks to support of The University of Akron and NASA Glenn Research Center grant NCC3-932 under the supervision of Gary D. Roberts. All impact tests were conducted at NASA Glenn ballistic laboratory under the guidance of J. M. Pereira and D. M. Revilock. Constructive suggestions of NASA Glenn personnel, in particular, K. Carney, C. Bowman, and R. Goldberg are appreciated. Input from General Electric Aircraft Engines engineers, in particular, M. Xie and M. Braley are also appreciated.

References

[1] Roberts, G. D., Pereira, J. M., Revilock, D. M., Binienda, W. K., Xie, M., and Braley, M., "Ballistic Impact of Braided Composites with a Soft Projectile," *Journal of Aerospace Engineering*, Vol. 18, No. 1, 2005, pp. 3–7.

[2] Cheng, J., Roberts, G. D., and Binienda, W. K., "Finite Element Simulation of Soft Projectiles Impacting Composites Targets," Society for the Advancement of Material and Process Engineering, Dayton, OH, 2003.

[3] *LSDYNA Keyword User's Manual*, Ver. 970, Livermore Software Technology Corp., Livermore, CA, 2004.

[4] Wilbeck, J. S., "Impact Behavior of Low Strength Projectiles," Ph.D. Dissertation, Texas A&M Univ., College Station, TX, 1977.

[5] Souli, M., Ouahsine, A., and Lewin, L., "ALE Formulation for Fluid-Structure Interaction Problems," *Computer Methods in Applied Mechanics and Engineering*, Vol. 190, Nos. 5–7, Nov. 2000, pp. 659–675.

[6] Schweizerhof, K., Weimar, K., and Rottner, T., "Crashworthiness Analysis with Enhanced Composite Material Models in LSDYNA: Merits and Limits," *Proceeding of Fifth LSDYNA International User Conference*, Livermore Software Technology Corp., Livermore, CA, Sept. 1998.

[7] Bowman, L., Roberts, G. D., Braley, M., Xie, M., and Booker, M., "Mechanical Properties of Triaxial Braided Carbon/Epoxy Composites," Society for the Advancement of Material and Process Engineering, Dayton, OH, 2003

[8] Jackson, W. C., and Poe, C. C., Jr., "The Use of Impact Force as a Scale Parameter for the Impact Response of Composite Laminates," NASA TM-104189, Jan. 1992.

[9] Kim, H., and Kedward, T., "Modeling Hail Ice Impacts and Predicting Impact Damage Initiation in Composite Structures," *AIAA Journal*, Vol. 38, No. 7, 2000, pp. 1278–1288.